Macromolecules

Article

pubs.acs.org/Macromolecules

Visualization of Individual Defect Mobility and Annihilation within Cylinder-Forming Diblock Copolymer Thin Films on Nanopatterned Substrates

Qianqian Tong and S. J. Sibener*

The James Franck Institute and Department of Chemistry, The University of Chicago, 929 E. 57th Street, Chicago, Illinois 60637, United States

ABSTRACT: We have tracked the mobility, approach, and annihilation of defects in cylinder-forming diblock copolymer thin films on nanopatterned substrates using high-temperature and *in situ* time-lapse atomic force microscopy. This has been accomplished by visualizing two isolated defects and studying their approach and hence interactions. Here we used lithographed channels to template and orientationally align cylindrical diblock domains macroscopically and with low defect density. Dislocation pairs annihilate through climb and glide motion, where climb is defined as a dislocation displacement along the diblock domain stripes, and glide is defined as dislocation motion across the stripes. Defect mobility via climbing motion is observed to be faster than glide excursions. The diffusion coefficients parallel (D_{par}) and perpendicular (D_{perp}) to the striped nanodomains have been determined; mobility along the cylinder direction is approximately 1 order of magnitude larger than that across the cylinders. Diffusion activation energies of both motions have been extracted from variable temperature measurements of defect mobility. Additionally, disclination pairs have been observed to annihilate by emission of dislocations and the topological switching of disclination cores. These measurements of single-defect mobility in otherwise perfected nanodomain regions allow for unusually precise determination of defect mobility and energetics for both dislocation and disclination pairs in nanoconfined polymer thin film systems.

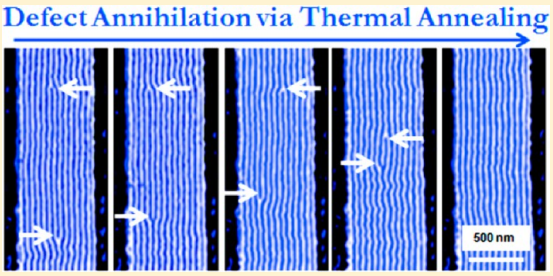

INTRODUCTION

Self-assembled systems have become increasingly valuable for the fabrication of nanoscale structures. Diblock copolymers are well-known examples of self-assembling systems. Thin films of these materials spontaneously form periodic microdomain structures of various symmetries, including spherical, cylindrical, and lamellar domains. These self-assembled patterns have been used as nanolithographic masks to create patterns on substrates[1−3] as well as templates for the further synthesis of metallic dots[4,5] and nanowires.[6,7] However, these applications require precise pattern registration and formation of long-range ordered nanostructures free from defects. Techniques that have been used to control the orientation of polymer domains and eliminate defects include electric fields,[8−10] flow fields,[11−13] directional crystallization,[14] chemical patterning,[15−19] and graphoepitaxy.[20−27] Graphoepitaxy utilizes the topography of the substrate to order microdomains. This technique was first used to achieve long-range order of spherical domains[20−22] and has since been used to align striped patterns of cylinder[23−26] or lamellae[27] forming block copolymers with both perpendicular and parallel orientations.

Many experimental studies have examined the pattern coarsening dynamics.[9,28−31] Figure 1 summarizes the types of the topological defects observed in the diblock copolymer thin films: disclocations (Figure 1a) and discliantions (Figure 1b). By tracking defects annihilation during annealing with time-lapse atomic force microscopy, Harrison et al.[29,30] showed that

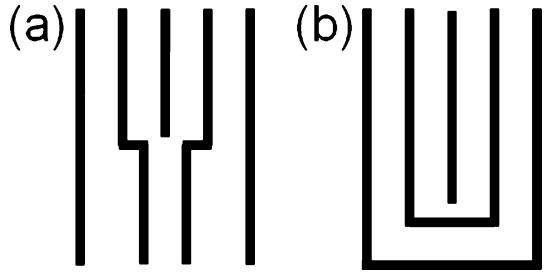

Figure 1. Schematics of typical topological defects in block copolymer systems: (a) elementary dislocation and (b) +1/2 disclination.

the coarsening process in cylinder-forming block copolymer thin films is dominated by disclination quadrupolar annihilation where the orientational correlation length obeys a power law with exponent $n = 1/4$. However, the detailed study of the dislocation and disclination motion is limited in their experimental works because of the poor time resolution and also the interacting strains from nearby defects. Simulation approaches have been demonstrated as powerful tools for the prediction of phase ordering in diblock copolymer systems. Avukhdeir et al. found that disclination motion requires the

Received: August 2, 2013
Revised: October 7, 2013
Published: October 25, 2013

absorption and emission of elementary dislocations, and the disclination lines act as a low-energy pathway for the movement.[32]

Pattern coarsening in diblock copolymers occurs by the motion of defects, which ultimately involves diffusion of polymer molecules. There is prior literature on the diffusion behavior in block copolymer systems.[33−38] In lamellar and cylinder systems, two self-diffusion coefficients can be defined: D_{par}, for diffusion along the interface, and D_{perp}, for diffusion across the interface. In an unentangled system, a block copolymer chain can diffuse freely parallel to the interface, while the diffusion perpendicular to the interface is retarded as a consequence of the repulsive interaction between the two immiscible blocks.[39,40] The anisotropy of diffusion, D_{par}/D_{perp}, was measured to be as large as 40 in poly(styrene-*b*-isoprene) lamellar systems by Hamersky et al.[36] Rittig et al.[37] investigated the diffusion behavior in a cylindrical PEP−PDMS diblock copolymer and found that the value of anisotropy diffusion D_{par}/D_{perp} deceases with temperature from 60 at 60 °C up to 5 at 195 °C. However, none of these studies connect polymer diffusion to pattern coarsening.

In this paper, we investigate the defect evolution of cylinder-forming PS-*b*-PMMA diblock copolymer thin films on nanopatterned substrates. Topographical templates allow us to align cylindrical domains macroscopically. In this way, we are able to isolate a pair of defects and to study their interactions and movement. Also, high-temperature imaging enables us to probe real-time and real-space defect evolution directly. We observe the climb and glide motions of dislocations and connect them to the diffusion of polymer chains for the first time, to our knowledge. Also, we probe the elementary steps of disclination quadrupole dynamics.

EXPERIMENTAL METHODS

A poly(styrene-*block*-methyl methacrylate) (PS-*b*-PMMA) block copolymer, obtained from Polymer Source, Inc. of Dorval, Quebec, was used in which PMMA forms cylindrical domains with a PS matrix. The molecular weight was 77 kg/mol with 29 wt % PMMA.

The silicon nitride substrates were spin-coated with a thin layer of PMMA photoresist and baked in air at 175 °C for more than an hour. A thin layer of Cr (70 Å) was then deposited onto the substrate using a homemade evaporator. The topographic patterns were prepared by electron beam lithography using a Hitachi S-2700 scanning electron microscope. After exposure, the films were developed in Cr etchant and then in a 1:3 mixture of methyl isobutyl ketone and isopropyl alcohol, rinsed extensively with isopropyl alcohol, and dried with nitrogen. The resulting patterns in the photoresist were converted into the topographic structures on the substrates by using a 95% CF_4 and 5% O_2 plasma etch. The remaining photoresist was removed by placing the substrates in acetone overnight. The nanochannels created in this manner are about 600 nm wide, 20 μm long and 50 nm deep. The nanopatterned substrates were cleaned with toluene, acetone, and methanol using an ultrasonic cleaner and dried with nitrogen. The washed substrates were spin-coated with PS-*b*-PMMA block copolymer in 0.9% toluene solution at 4000−5500 rpm for 60 s and then preannealed at 523 K for 2.5 h under an argon atmosphere.

The samples were imaged in the high-temperature closed cell of Asylum Research's MFP-3D AFM under room-temperature argon flow. Imaging was performed in ac (tapping) mode, using Olympus AC240TS cantilevers with a spring constant of 2 N/m. The drive frequency and the amplitude set point differ from cantilever to cantilever. However, we used the smallest tapping force as required to obtain a clear image in order to avoid perturbing influences from the cantilever tips on the diffusion of the polymer melt. All AFM imaging were performed in the repulsive regime with scanning rate ranges from 2 to 4 Hz.

Asymmetric wetting of PS-*b*-PMMA occurs on the nanopatterned silicon nitride substrate. PMMA favors the silicon nitride substrate because of its lower wetting energy. At the polymer/air interface, the surface tension difference between PMMA and PS is small enough to produce the appearance of both components at the upper interface. The crests appear featureless, corresponding to an $L/2$ thick film, where L is the natural thickness of one layer of cylinders. The troughs are filled with a layer of PMMA cylinders, which show fingerprint structures.

RESULTS AND DISCUSSION

Dislocation Annihilation Mechanism: Climb and Glide. Two dislocations with opposite signs will attract and eventually annihilate with each other. Dislocation annihilation proceeds with climb and glide. Climb describes a dislocation motion along the stripes, while glide describes the motion across the stripes. For smectic A and columnar systems, glide is predicted to be more difficult than climb, since glide involves interdiffusion across the interface and mixing of two blocks.[41,42] However, it has not been verified experimentally, as far as we know, due to the difficulty of distinguishing climb and glide on randomly oriented polymer thin films.[30] Our cylinder-forming block copolymer has the columnar symmetry. Topographical templates allow us to direct the orientation of polymer domains, and the resulting long-range alignment with low defect densities and straight domains enables us to isolate a pair of dislocations and to study their interactions and movements. Moreover, in situ high-temperature AFM imaging enables us to quantitatively study the climb and glide motions of dislocations and link them to the diffusion of polymer chains for the first time.

An example of climb motion is shown in Figure 2a. The AFM images are taken at 240 °C, and the time interval between two subsequent images is about 3 min. Climb motion is inevitably accompanied by glide motion. However, here the separation in the climb direction is much larger than that in the glide direction, so we can neglect the separation distance in the glide direction. At t = 0, a pair of dislocations with opposite Burgers vector is 2.4 μm apart from each other. The attractive interaction causes the two dislocations to approach. Thus, the separation distance decreases with the annealing time. After about 15 min of annealing, the distance between the two dislocation cores is reduced to 1.7 μm. The attractive interaction continues to cause the reduction of the separation distance. Eventually, at t = 36 min 35 s, the dislocation pair annihilates, leaving a defect-free region. In Figure 2b, the distance between the cores of the two dislocations r is shown as a function of time. The force between two dislocations F_{ds} decreases with the separation distance as $F_{ds} \approx \mu d_0^2/[2\pi(1-\nu)r] \propto 1/r$, where μ is the shear modulus of the polymer, ν is Poisson's ratio, and d_0 is the natural spacing of cylinder domains.[43−46] If we assume that the dislocation motion is viscous with a velocity proportional to force, the velocity scales with separation distance as $-(dr/dt) \propto 1/r$, yielding $r^2 \propto (t_f - t)$, where t_f is the annihilation time of the pair of dislocations.[44,46,47] Our data are found to be consistent with this power law dependence, as shown in Figure 2b.

Moreover, climb occurs by diffusion of polymer molecules parallel to the striped layers. According to the Einstein relation $x^2 = 2Dt$, where x is the one-dimensional displacement and D is the diffusion coefficient. By assuming that each one of the two dislocations moves half the distance between them, each dislocation moves a distance of $r/2$ within the time interval of $(t_f - t)$. Therefore, $(r/2)^2 = 2D_{par}(t_f - t)$. From the slope of the

dx.doi.org/10.1021/ma401629s | Macromolecules 2013, 46, 8538−8544

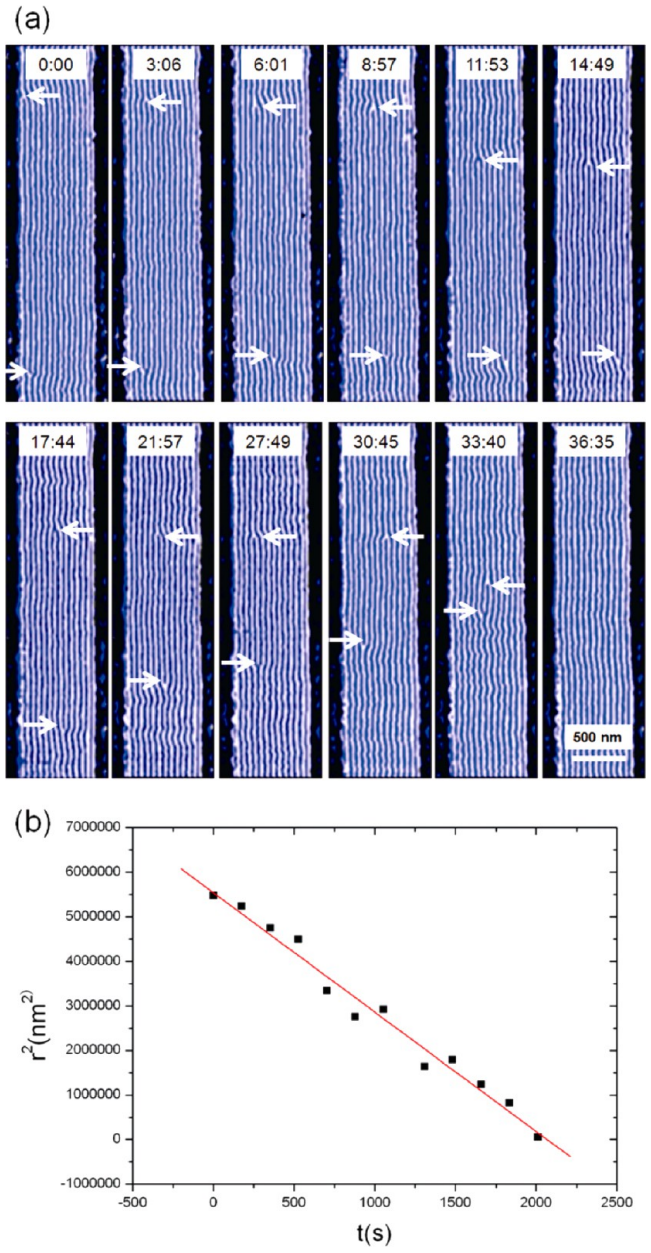

Figure 2. (a) Time sequence of AFM phase images showing climb motion of two dislocations of opposite Burgers vectors. The two dislocation cores are indicated by the arrows. The number at the top of each image indicates the time when the image is taken. The images are taken at 240 °C. (b) The square of the distance between the two dislocation cores is plotted corresponding to the time for the images shown in (a).

line in Figure 2b, the parallel diffusion coefficient D_{par} is calculated to be 3.0×10^{-12} cm^2/s, and D_{par} is determined to be $(2.6 \pm 0.5) \times 10^{-12}$ cm^2/s by averaging the diffusion coefficients of five pairs of dislocations at 240 °C. The spread of the value stems from the sensitivity of the self-diffusion coefficient to defects even in the nominally "perfectly aligned" regions.[38] Previously, Milhaupt et al. measured the diffusion coefficients and viscosity of disordered PS-*b*-PMMA.[48] Using their Williams–Landel–Ferry (WLF) parameters, extrapolating to the temperature of 240 °C and scaling to our molecular weight, the self-diffusion coefficient for PS-*b*-PMMA with 68 wt % PS is determined to be 2.8×10^{-12} cm^2/s from their viscosity measurements and 4.2×10^{-11} cm^2/s from their diffusion measurement, which compares well with our results given the combined uncertainties.

The diffusion of a chain is subject to the friction of either block. Climb will take place spontaneously if the attraction between two oppositely oriented dislocations F_{climb} outweighs the diffusion barrier, E_A. Therefore, the critical distance (R^*) for annihilation of dislocations is thus given by[41,49]

$$F_{climb} \approx \frac{\mu {d_0}^2}{2\pi(1-\nu)R^*} \geq \frac{E_A}{N_A {d_0}^2} \quad (1)$$

Here we ignore the bend deformation of cylinders and use the climb force in crystal solids to roughly estimate the critical distance. We take μ as 10^{-3} GPa,[50] ν as 0.5,[49] d_0 as 50 nm, and E_A as 270 kJ/mol.[51] The critical distance R^* is estimated to be ~4 μm, which is larger than the initial separation distance of the dislocation pairs in our experiments. Therefore, the climb of the dislocation pairs is indeed driven by their attractive interactions.

In contrast to climb, glide motion is much slower. An example of glide motion is shown in Figure 3a. At t = 0, the two

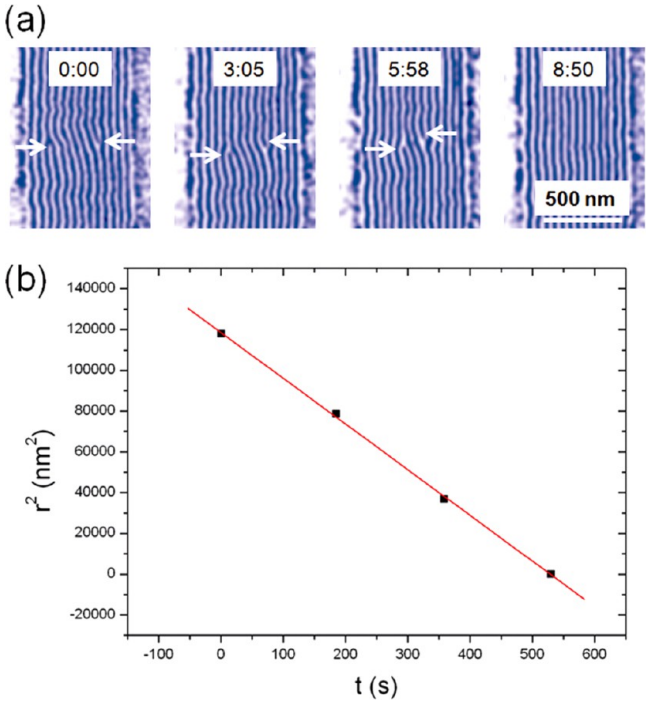

Figure 3. (a) Time sequence of AFM phase images showing glide motion of two dislocations of opposite Burgers vectors. The dislocation cores are indicated by the arrows. The number at the top of each image indicates the time when the image was taken. The images are taken at 240 °C. (b) The square of the distance between the two dislocation cores is plotted to the time for the images shown in (a).

oppositely oriented dislocations are separated by 7 layers. After annealing for about 3 and 6 min, the separation distances are reduced to 5 and 3 layers, respectively. Finally, the two dislocations collide and annihilate at t = 8 min 50 s, leaving a defect-free region. Glide occurs by collective diffusion of molecules perpendicular to the striped layers. The distance between the cores of the two dislocations r is consistent with the power law dependence $r^2 \propto (t_f - t)$, as shown in Figure 3b. In the same manner as we obtained D_{par}, the perpendicular

dx.doi.org/10.1021/ma401629s | Macromolecules 2013, 46, 8538–8544

diffusion coefficient D_{perp} is determined to be $(3.2 \pm 0.4) \times 10^{-13}$ cm^2/s, which is an order of magnitude smaller than D_{par}. As expected, climb is faster than glide because glide necessitates mixing of two blocks. If an individual polymer chain propagates in a way that its PMMA block moves from one cylinder domain to another, this block copolymer chain must pass through a matrix consisting of PS block. Green studied the tracer diffusion of PS-*b*-PMMA diblock copolymer into PS homopolymer.[52] Using his model, the diffusion coefficient of PS-*b*-PMMA (55K-*b*-22K) diblock into PS homopolymer is calculated to be 10^{-13} cm^2/s at 240 °C, which compares well with our value of the perpendicular diffusion coefficient. Our results are also consistent with the D_{perp} value of 10^{-13} cm^2/s estimated from the rapid opening and closing of a connection between cylindrical domains of SB block copolymer melts.[53]

Previous work by Ruiz et al. studied the coarsening kinetics in lamellar- and cylinder-forming block copolymer thin films.[51] They argued that glide can only occur by interdiffusion across the interface in the lamellar phase. However, in the cylinder phase, glide can be achieved by either perpendicular diffusion of molecules or rotation around the cylinder cores, which is associated with D_{par}. The difference between the two systems results from the interconnected matrix present in cylindrical-phase polymers. Unfortunately, we could not see how glide motion occurs at the molecular level from our AFM images. However, our results show that glide mobility, in cylinder-forming block copolymer thin films, is indeed 1 order of magnitude slower than climb rate, which indicates glide motion is dominated by perpendicular diffusion of molecules. Whether glide motion is also associated with parallel diffusion can be determined after studying the glide mobility in lamellar-forming block copolymer thin films. Although the diffusion behavior in lamellar structures is beyond the scope of this article, it is of great interest and will be pursued in the future.

Anisotropy of Diffusion D_{par}/D_{perp} and Activation Energies for Diffusion. We now discuss the temperature dependence of the diffusion coefficients. Measurements of D_{par} and D_{perp} were also conducted at 238, 242, and 244 °C. The results are plotted in Figure 4 along with the results measured at 240 °C. The anisotropy of diffusion D_{par}/D_{perp} decreases from 9 at 238 °C to 7 at 244 °C. The recent simulation work by Chang et al. calculated the anisotropy of diffusion for cylinder-forming PS-*b*-PMMA block copolymer with different segregation strength χN,[54] where χ is the Flory–Huggins parameter and N is the number of statistical segments. By taking $\chi(T)$ as $0.021 + 3.20/T$,[55] the polymer used in this study has a χN of ~21. The anisotropy of diffusion is predicted to be ~10 with $\chi N = 21$, which is in good agreement with our results. The observed temperature dependence of diffusion coefficients follows an Arrhenius law with the activation energy of $E_{a,par} = 127 \pm 59$ kJ/mol and $E_{a,perp} = 214 \pm 74$ kJ/mol for parallel and perpendicular diffusion, respectively. The deviation results from the limited temperature range in our experiment. These values compare well with previous measurement of 377 kJ/mol for diffusion in cylinder-forming films of PS-*b*-PMMA with M_n = 84 kg/mol[31] and 270 kJ/mol for PS-*b*-PMMA with M_n = 64 kg/mol.[51]

Next, we compare our temperature dependence of D_{par} to previous viscosity measurements. The temperature behavior of viscosity is well described by the "WLF equation", stating

$$\log \frac{\eta(T)}{\eta(T_{ref})} = \log a_T = \frac{-C_1(T - T_{ref})}{C_2 + (T - T_{ref})} \quad (2)$$

where η is the steady shear viscosity, T_{ref} is the reference temperature, a_T is the temperature shift factor, and C_1 and C_2 are WLF parameters. In general, the WLF equation holds in the temperature range T_g to T_g + 100 °C. However, Scheer et al. have proven its applicability up to 250 °C for both PS and PMMA.[56] Since the reduced diffusion coefficient D/T is inversely proportional to viscosity η,[57] the temperature shift factor a_T can also be determined from diffusion coefficient by[57,58]

$$\log a_T = \log \frac{D(T_{ref})T}{DT_{ref}} \quad (3)$$

where $D(T_{ref})$ is the self-diffusion coefficient at the reference temperature. The temperature shift factor a_T is plotted in Figure 5 with a reference temperature taken to be T_{ref} = 240 °C. The dots correspond to those determined from our D_{par} and the curves correspond to those determined from previous

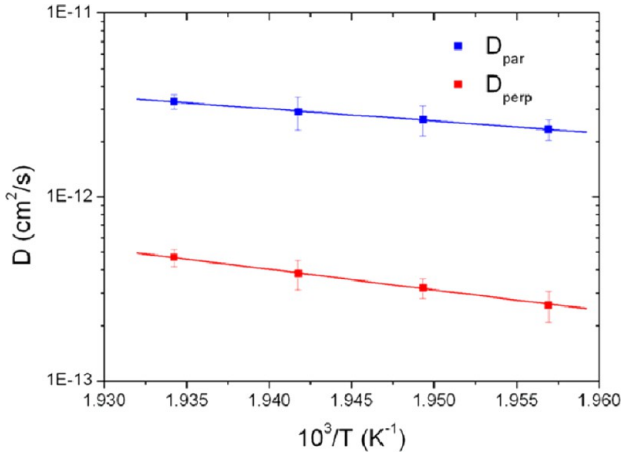

Figure 4. Arrhenius plot of the diffusion coefficient D_{par} (blue) and D_{perp} (red) of the diblock copolymer. The activation energy for parallel and perpendicular diffusion are determined to be $E_{a,par} = 127 \pm 59$ kJ/mol and $E_{a,perp} = 214 \pm 74$ kJ/mol, respectively.

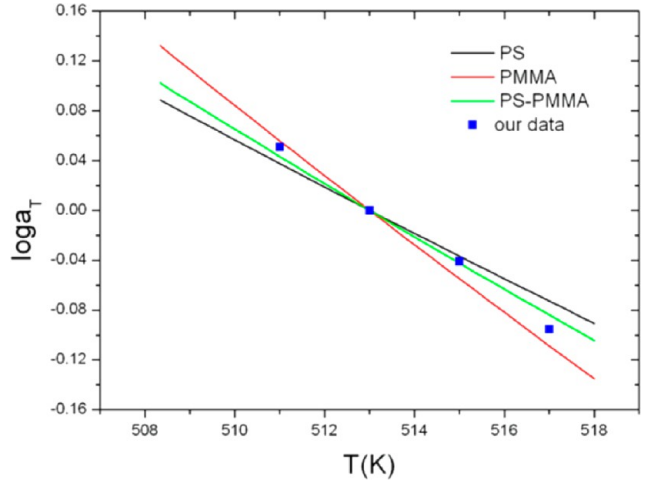

Figure 5. Temperature shift factors as obtained from diffusion measurements (dots) as well as from previous viscosity measurements (curves). The shift factors are given for a reference temperature of 240 °C.

dx.doi.org/10.1021/ma401629s | Macromolecules 2013, 46, 8538–8544

shear viscosity measurements. The black and red lines are obtained using the best fit WLF parameters from Scheer et al. for PS and PMMA, respectively.[56] Our temperature shift factor a_T for PS-*b*-PMMA is between the values for pure PS and pure PMMA, which is reasonable since the diffusion of a chain along the domain is subjected to the monomeric friction of both blocks. Consistency between diffusion derived a_T for block copolymer and a_T from viscosity for PS-*b*-PMMA is observed. The green line is obtained using the WLF parameter from Milhaupt et al. for 15.7 kg/mol PS-*b*-PMMA with 68 wt % PS.[48] Our a_T has a slightly larger temperature dependence than theirs, which may result from their low molecular weight. It has been shown that below the molecular weight of 30 kg/mol, $\partial \ln a_T/\partial T$ decreases as the molecular weight decreases, due to the an enhanced free volume associated with the ends of molecules.[59] In general, our values of a_T from D agree well with previous results from η. Besides, the temperature shift factor a_T compensates for the temperature dependence of single-chain mobility. The agreement of a_T suggests that the movement of defects ultimately involves the motion of single polymer chains, which is consistent with Amundson et al.[60]

As stated above, in addition to friction barrier, the motion perpendicular to the cylinder axis is further retarded by the repulsive interaction between the two immiscible blocks. When a PMMA block moves from one PMMA domain to another, it has to pass through a matrix consisting of PS chains. Thus, the diblock copolymer has to pass an energy barrier scales as χN_A, corresponding to the enthalpic price for placing the PMMA block in the PS domain.

Therefore[35,61]

$$D_{perp} \approx D_0 e^{-\alpha \chi N_A} \quad (4)$$

where D_0 is the self-diffusion coefficient in the disordered, homogeneous systems, α is a material parameter of order unity, χ is the Flory–Huggins parameter, and N_A is the degree of polymerization of the block infiltrating the unfavorable domains. For the nonentangled block copolymers, $D_{par} \approx D_0$.[38,51] For entangled systems, the block copolymer chains can not simply diffuse along the interfaces without pulling the A block into the B-rich domain due to the entanglement. Therefore, D_{par}/D_0 follows an exponential dependence on χN.[34,38] The critical molar mass M_c is 30 kg/mol for PMMA and 35 kg/mol for PS.[62] Therefore, the only slightly entangled block in our experiment is PS block. However, it has been shown that the effect of this slight entanglement on the parallel diffusion coefficients is not apparent and can be ignored.[51] Hence, we use D_{par} as D_0. Using eq 4, α is determined to be 0.33–0.36 for the four temperatures studied. These values are comparable to what was found before: α = 1/3 for cylindrical PS–PB diblock copolymer,[53] α = 0.33–0.46 for cylindrical PEP–PDMS diblock copolymer,[37] and α = 0.5 for cylindrical PEO–PEE diblock copolymer.[35] Such agreement further indicates that the anisotropy of diffusion is attributed to the thermodynamic penalty for mixing of the two blocks.

Disclination Annihilation. Previous experimental work by Harrison et al. showed that pattern coarsening in a cylinder-forming block copolymer thin film is dominated by disclination quadrupolar interactions.[29] The attractive force between two oppositely oriented disclinations has the form $F = 2\pi k_1 k_2 K_1/r$, where r is the distance between two disclination cores, k_1 and k_2 are the winding number of the defects (here +1/2 and −1/2, respectively), and K_1 is the splay elastic coefficient. However, the disclinations cannot simply move in response to the forces because of the topological constraint imposed on them in the striped phase. Here, the time-lapse AFM images at high temperature enable us to investigate how domains break and rejoin in order for the disclinations to move and annihilate.

Figure 6a is the time sequence of AFM images tracking disclination quadrupolar annihilation. At t = 0, two disclinations

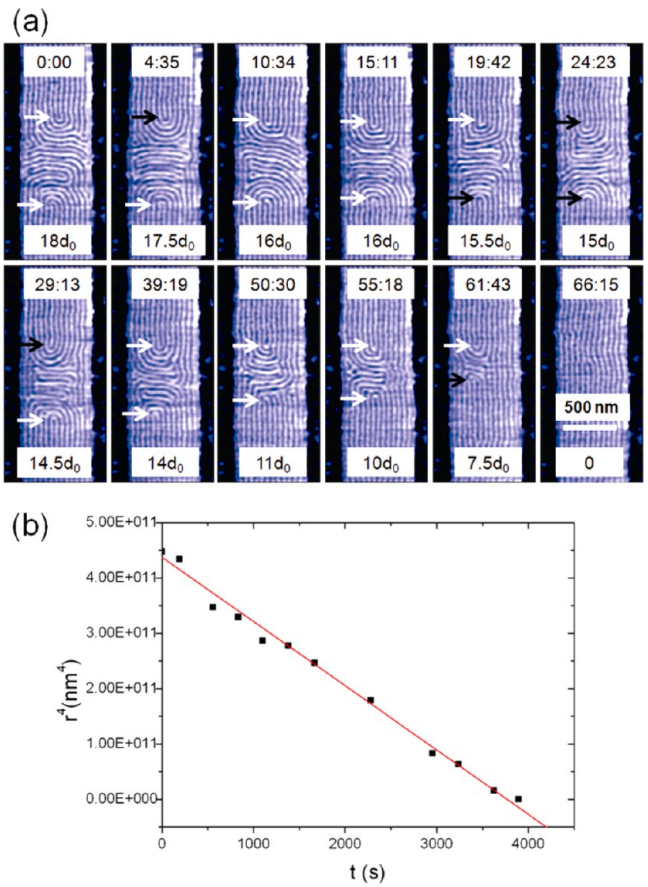

Figure 6. (a) Time sequence of AFM images showing annihilation of a disclination quadrupole. The number at the top indicates the time that the image is taken, and the number at the bottom of each image indicates the spacing between the two disclination cores. The white arrow corresponds to the PMMA disclination core, while the black arrow corresponds to the PS disclination core. The images are taken at 240 °C. (b) The distance between the two disclination cores is plotted to the fourth power as a function of time for the images shown in (a).

with oppositely oriented Burgers vectors are separated by 18 layers. After a 30 min anneal at 240 °C, the disclination core spacing is reduced to 14.5d_0. The nonintegral distance results from the different core types of the two disclinations: the upper one consists of a PS core; the lower one consists of a PMMA core. As the separation distance becomes smaller, the attractive force between the disclination pair will be stronger, and the velocities of disclinations will become faster. Finally, at t = 66 min 15 s, the two disclinations annihilate, leaving a pair of oppositely charged dislocations. The spacing between the two disclinations as a function of annealing time is plotted in Figure 6b. The straight line indicates consistency with the proposed $t^{1/4}$ power law.[29]

Figure 7a–e is a series of AFM images at intermediate times in the coarsening process of Figure 6a where two oppositely oriented disclinations move toward each other. In panel a, two

dx.doi.org/10.1021/ma401629s | Macromolecules 2013, 46, 8538–8544

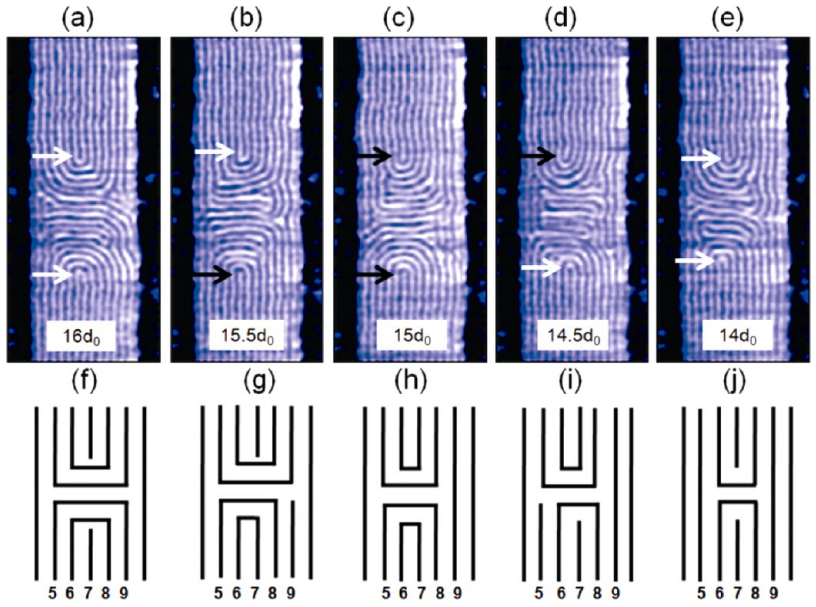

Figure 7. (a–e) Representative AFM images taken from the sequence in Figure 6a showing breaking and relinking processes of a disclination pair. The white arrow corresponds to the PMMA disclination core, while the black arrow corresponds to the PS disclination core. The number at the bottom of each image indicates the spacing between the two disclination cores. By emission of the disclination lines into dislocations and the alternation of the disclination cores, the two disclinations move toward each other. (f–j) Schematic of the quadrupole mechanism of (a–e). For simplicity, only disclination core regions are drawn. The dark lines correspond to the disclination lines, and the numbers below are the sequence numbers of disclination lines of the lower disclination in (a–e).

disclinations are separated by 16 layers, and both disclinations consist PMMA cores. The separation distance is decreased to 15.5 layers in the next image, and the lower disclination switches to a PS core. The separation distance is 15 layers in panel c, where both disclinations have PS cores. The separation distance continues to decrease in panels d and e.

The annihilation process is schematicized in Figure 7f–j. For simplicity, only disclination core regions are drawn. The dark lines correspond to the disclination lines, and the numbers below are sequence numbers of disclination lines of the lower disclinations in panels a–e. For example, in panel f, the second dark line to the left is the fifth disclination line of the lower disclination in panel a counting from left to right. At first, the fifth line is connected to the ninth line, and the sixth line is connected to the eighth line. The seventh line is the disclination core. In panel g, which is a schematic illustration of panel b, the fifth line is reconnected to the eighth line, and the sixth line is reconnected to the seventh line. The ninth line is emitted from the disclination, and forms a dislocation. The core of the lower disclination switches from dark (PMMA) core to light (PS) core. The result of this process is the emission of a dislocation and the separation distance between two disclinations decreased by 1/2 layer. In panel h, similar breaking and relinking is observed in the upper disclination. The core of the upper disclination switches from dark to light, and the distance between the two disclinations is further decreased by 1/2 layer. The dislocation emitted is free to interact. In panel i, for the lower disclination, the sixth line is relinked to the eighth line, and the fifth line is emitted to be a dislocation. The disclination core switches back to a PMMA core, and the separation distance between the two disclinations is further decreased by 1/2 layer. In panel j, the core of the upper disclination switches from light to dark by emission of a dislocation. Now, both of the two disclinations have dark cores, the same core structures as in panel f, but the separation distance between them is reduced by 2 layers compared to panel f. This process will repeat until annihilation of the disclinations. By emission of the disclination lines into dislocations and the alternation of the disclination cores, the disclinations are able to approach each other. Our results are in superb agreement with previous simulations, which also show that the movement of each disclination involves the absorption or emission of an elementary dislocation and a transition of the core of the disclination.[32]

CONCLUSION

We have observed *in situ* defect evolution and annihilation of diblock copolymer thin films on nanopatterned substrates directly, using high temperature time-lapse AFM imaging with environmental control. Topographical templates direct the orientation of polymer domains macroscopically, which enables us to isolate a defect pair and to study their interactions. Dislocations are found to annihilate by climb and glide, where climb is defined as a dislocation displacement along the stripes and glide is defined as dislocation motion across the stripes. Climb is faster than glide, since glide requires interdiffusion across the interface and mixing of two blocks. By tracking the annihilation of dislocation pairs, D_{par} and D_{perp} are obtained, and the anisotropy of diffusion D_{par}/D_{perp} is found to be about 10 for the temperatures we studied. The activation energies are also determined for both diffusion paths. Additionally, the motion of disclinations is found to be through emission of disclination lines into dislocations and switching of the disclination cores.

AUTHOR INFORMATION

Corresponding Author

*E-mail: s-sibener@uchicago.edu (S.J.S.).

Notes

The authors declare no competing financial interest.

■ ACKNOWLEDGMENTS

This work was supported by DTRA under Grant HDTRA1-11-1-0001. It is also a pleasure to acknowledge partial support from the Materials Research Science and Engineering Center at The University of Chicago, NSF-DMR-0820054.

■ REFERENCES

(1) Park, M.; Harrison, C.; Chaikin, P. M.; Register, R. A.; Adamson, D. H. *Science* **1997**, *276*, 1401−1404.
(2) Rachel, A. S. *Mater. Sci. Eng., R* **2005**, *48*, 191−226.
(3) Park, C.; Yoon, J.; Thomas, E. L. *Polymer* **2003**, *44*, 6725−6760.
(4) Sohn, B. H.; Seo, B. H. *Chem. Mater.* **2001**, *13*, 1752−1757.
(5) Watkins, J. J.; McCarthy, T. J. *Chem. Mater.* **1995**, *7*, 1991−1994.
(6) Kim, H. C.; Jia, X.; Stafford, C. M.; Kim, D. H.; McCarthy, T. J.; Tuominen, M.; Hawker, C. J.; Russell, T. P. *Adv. Mater.* **2001**, *13*, 795−797.
(7) Thurn-Albrecht, T.; Schotter, J.; Kästle, G. A.; Emley, N.; Shibauchi, T.; Krusin-Elbaum, L.; Guarini, K.; Black, C. T.; Tuominen, M. T.; Russell, T. P. *Science* **2000**, *290*, 2126−2129.
(8) Thurn-Albrecht, T.; DeRouchey, J.; Russell, T. P.; Kolb, R. *Macromolecules* **2002**, *35*, 8106−8110.
(9) Amundson, K.; Helfand, E.; Quan, X.; Hudson, S. D.; Smith, S. D. *Macromolecules* **1994**, *27*, 6559−6570.
(10) Morkved, T. L.; Lu, M.; Urbas, A. M.; Ehrichs, E. E.; Jaeger, H. M.; Mansky, P.; Russell, T. P. *Science* **1996**, *273*, 931−933.
(11) Angelescu, D. E.; Waller, J. H.; Adamson, D. H.; Deshpande, P.; Chou, S. Y.; Register, R. A.; Chaikin, P. M. *Adv. Mater.* **2004**, *16*, 1736−1740.
(12) Kimura, M.; Misner, M. J.; Xu, T.; Kim, S. H.; Russell, T. P. *Langmuir* **2003**, *19*, 9910−9913.
(13) Petermann, J.; Gohil, R. M. *J. Mater. Sci.* **1979**, *14*, 2260−2264.
(14) Park, C.; De Rosa, C.; Thomas, E. L. *Macromolecules* **2001**, *34*, 2602−2606.
(15) Chen, H. *J. Chem. Phys.* **1998**, *108*, 6897.
(16) Pereira, G. G.; Williams, D. R. M. *Macromolecules* **1999**, *32*, 758−764.
(17) Rockford, L.; Liu, Y.; Mansky, P.; Russell, T. P.; Yoon, M.; Mochrie, S. G. J. *Phys. Rev. Lett.* **1999**, *82*, 2602−2605.
(18) Kim, O. S.; Solak, H. H.; Stoykovich, M. P.; Ferrier, N. J.; de Pablo, J. J.; Nealey, P. F. *Nature* **2003**, *424*, 411−414.
(19) Park, S.-M.; Craig, G. S. W.; Liu, C.-C.; La, Y.-H.; Ferrier, N. J.; Nealey, P. F. *Macromolecules* **2008**, *41*, 9118−9123.
(20) Segalman, R. A.; Yokoyama, H.; Kramer, E. J. *Adv. Mater.* **2001**, *13*, 1152−1155.
(21) Segalman, R. A.; Hexemer, A.; Kramer, E. J. *Phys. Rev. Lett.* **2003**, *91*, 196101.
(22) Segalman, R. A.; Hexemer, A.; Kramer, E. J. *Macromolecules* **2003**, *36*, 6831−6839.
(23) Sundrani, D.; Darling, S. B.; Sibener, S. J. *Nano Lett.* **2003**, *4*, 273−276.
(24) Kim, S. H.; Misner, M. J.; Xu, T.; Kimura, M.; Russell, T. P. *Adv. Mater.* **2004**, *16*, 226−231.
(25) Black, C. T.; Bezencenet, O. *IEEE Trans. Nanotechnol.* **2004**, *3*, 412−415.
(26) Sundrani, D.; Darling, S. B.; Sibener, S. J. *Langmuir* **2004**, *20*, 5091−5099.
(27) Park, S. M.; Stoykovich, M. P.; Ruiz, R.; Zhang, Y.; Black, C. T.; Nealey, P. F. *Adv. Mater.* **2007**, *19*, 607−611.
(28) Hahm, J.; Lopes, W. A.; Jaeger, H. M.; Sibener, S. J. *J. Chem. Phys.* **1998**, *109*, 10111−10114.
(29) Harrison, C.; Adamson, D. H.; Cheng, Z.; Sebastian, J. M.; Sethuraman, S.; Huse, D. A.; Register, R. A.; Chaikin, P. M. *Science* **2000**, *290*, 1558−1560.
(30) Harrison, C.; Cheng, Z.; Sethuraman, S.; Huse, D. A.; Chaikin, P. M.; Vega, D. A.; Sebastian, J. M.; Register, R. A.; Adamson, D. H. *Phys. Rev. E* **2002**, *66*, 011706.
(31) Hahm, J.; Sibener, S. J. *J. Chem. Phys.* **2001**, *114*, 4730−4740.
(32) Nasser Mohieddin Abukhdeir; Alejandro, D. R. *New J. Phys.* **2008**, *10*, 063025.
(33) Dalvi, M. C.; Lodge, T. P. *Macromolecules* **1993**, *26*, 859−861.
(34) Lodge, T. P.; Dalvi, M. C. *Phys. Rev. Lett.* **1995**, *75*, 657−660.
(35) Hamersky, M. W.; Hillmyer, M. A.; Tirrell, M.; Bates, F. S.; Lodge, T. P.; von Meerwall, E. D. *Macromolecules* **1998**, *31*, 5363−5370.
(36) Hamersky, M. W.; Tirrell, M.; Lodge, T. P. *Langmuir* **1998**, *14*, 6974−6979.
(37) Rittig, F.; Fleischer, G.; Kärger, J.; Papadakis, C. M.; Almdal, K.; Štěpánek, P. *Macromolecules* **1999**, *32*, 5872−5877.
(38) Cavicchi, K. A.; Lodge, T. P. *Macromolecules* **2004**, *37*, 6004−6012.
(39) Ehlich, D.; Takenaka, M.; Okamoto, S.; Hashimoto, T. *Macromolecules* **1993**, *26*, 189−197.
(40) Ehlich, D.; Takenaka, M.; Hashimoto, T. *Macromolecules* **1993**, *26*, 492−498.
(41) Kleman, M.; Williams, C. E. *J. Phys., Lett.* **1974**, *35*, 49−51.
(42) Kleman, M.; Lavrentovich, O. D. *Soft Matter Physics: An Introduction*; Springer: New York, 2002; pp 300−336.
(43) Goren, G.; Procaccia, I.; Rasenat, S.; Steinberg, V. *Phys. Rev. Lett.* **1989**, *63*, 1237−1240.
(44) Pezzutti, A. D.; Vega, D. A.; Villar, M. A. *Philos. Trans. R. Soc., A* *369*, 335−350.
(45) Amodeo, R. J.; Ghoniem, N. M. *Phys. Rev. B* **1990**, *41*, 6958−6967.
(46) Tsimring, L. S. *Phys. Rev. Lett.* **1995**, *74*, 4201−4204.
(47) Ambrožič, M.; Kralj, S.; Sluckin, T. J.; Žumer, S.; Svenšek, D. *Phys. Rev. E* **2004**, *70*, 051704.
(48) Milhaupt, J. M.; Lodge, T. P.; Smith, S. D.; Hamersky, M. W. *Macromolecules* **2001**, *34*, 5561−5570.
(49) Friedel, J. *Dislocations*. Reprinted with corrections ed.; Pergamon; Distributed in USA by Addison-Wesley Pub. Co.: Oxford Reading, MA, 1964; p 104.
(50) Lach, R.; Grellmann, W.; Schröter, K.; Donth, E. *Polymer* **1999**, *40*, 1481−1485.
(51) Ruiz, R.; Bosworth, J. K.; Black, C. T. *Phys. Rev. B* **2008**, *77*, 054204.
(52) Green, P. F. *Macromolecules* **1995**, *28*, 2155−2158.
(53) Tsarkova, L.; Knoll, A.; Magerle, R. *Nano Lett.* **2006**, *6*, 1574−1577.
(54) Chang, S.-w.; Evans, J. P.; Ge, S.; Ginzburg, V. V.; Kramer, J. W.; Landes, B.; Lee, C.; Meyers, G. F.; Murray, D. J.; Park, J.; Sharma, R.; Trefonas, P.; Weinhold, J. D.; Zhang, J.; Hustad, P. D. *Proc. SPIE* **2013**, *8680*, 86800F-1−86800F-9.
(55) Russell, T. P. *Macromolecules* **1993**, *26*, 5819−5819.
(56) Scheer, H. C.; Bogdanski, N.; Wissen, M.; Möllenbeck, S. *Microelectron. Eng.* **2008**, *85*, 890−896.
(57) Mumby, S. J.; Smith, B. A.; Samulski, E. T.; Yu, L.-P.; Winnik, M. A. *Polymer* **1986**, *27*, 1826−1828.
(58) Shearmur, T. E.; Clough, A. S.; Drew, D. W.; van der Grinten, M. G. D.; Jones, R. A. L. *Polymer* **1998**, *39*, 2155−2159.
(59) Ferry, J. D. *Viscoelastic Properties of Polymers*; Wiley: New York, 1961; p 482.
(60) Amundson, K.; Helfand, E.; Quan, X.; Smith, S. D. *Macromolecules* **1993**, *26*, 2698−2703.
(61) Rittig, C. M. P. A. F. *J. Phys.: Condens. Matter* **2005**, *17*, R551.
(62) Graessley, W. W. *The Entanglement Concept in Polymer Rheology*; Springer: Berlin, 1975; Vol. *18*, p 151.